**RESEARCH PAPER**

# Efficient prediction of residual stress in additive manufacturing based on semi-analytical solution

**Maohong Yang[1,2] · Guiyi Wu[1] · Xiangwei Li[1] · Ruiyao Zhang[1] · Shuyan Zhang[1] · Honghong Wang[2]**

## Abstract

In order to improve the efficiency of residual stress simulation in laser powder feeding additive manufacturing, a finite element modeling method that only requires to solve the stress field is proposed and established in this paper. First, the analytical solution of the heat conduction equation is simplified, and a new temperature field model is developed, which can be directly input into the stress field model for calculation, thereby eliminating the calculation of the temperature field in the thermal–mechanical coupling simulation process and improving the simulation efficiency of residual stress in additive manufacturing. On this basis, the effectiveness of the method is verified by a single-pass single-layer cladding simulation. Meanwhile, the residual stress of single-pass multi-layer cladding is calculated and compared with the measured results, and the distribution characteristics of residual stress in additive manufacturing are studied. It is demonstrated that the result of the established model is closed to that of thermal–mechanical coupled finite element method. The established model can reflect the residual stress of laser powder feeding additive manufacturing process. Compared with the traditional thermal–mechanical coupled finite element method, the computational efficiency of the model established in this study is greatly improved.

**Keywords** Temperature field model · Residual stress · Laser powder feeding additive manufacturing · Calculation efficiency

## 1 Introduction

Selective laser melting (SLM) is an additive manufacturing (AM) method based on laser sintering metal powders to produce metal parts with complex topologies by depositing material layer by layer. During the forming process, layer-by-layer cladding of material results in temperature gradients and changes in cooling rates, which induce residual stresses. These stresses may lead to deformation of components, crack growth and reduction of fatigue life, thereby affecting the reliability and service life of components. The deformation and residual stress of additively manufactured parts are

the main challenges for the large-scale application of AM [1–6]. Rapid and accurate prediction of the residual stress in the SLM process will help to reduce the deformation of components, and a deep understanding of the mechanism of component cracking is of great significance to the application of SLM [7, 8].

Thermal–mechanical coupling analysis using finite element method is one of the ways to predict residual stress in additive manufacturing. At present, there are two main research directions in the residual stress simulation of additive manufacturing. The first is to further consider various physical and metallurgical phenomena in the actual forming process to make the predicted residual stress more accurate. In order to improve the accuracy of calculation, Chen, Weisz-Patrault, and Ahn et al. [9–11] developed finite element models including thermal strain caused by temperature gradient change, phase transition stress caused by solid phase transition, and residual stress caused by mechanical constraints, respectively. Mirkoohi et al. [12] incorporated dynamic recrystallization and grain size into the finite element model, and the established model can predict the effect of grain refinement on residual stress. Mukherjee et al. [13],

✉ Guiyi Wu
guiyi.wu@ceamat.com

1  Centre of Excellence for Advanced Materials, Dongguan 523808, China

2  School of Materials and Metallurgy, Wuhan University of Science and Technology, Wuhan 430081, China

Falla et al. [14], Walker et al. [15] and Wolff et al. [16] considered the molten pool convection in the residual stress model and the effect of molten pool convection on residual stress is studied. However, the more complex the physical process considered, the lower the solution efficiency of the model will be, and even some large-scale AM components may be impossible to solve. Therefore, improving the computational efficiency of the model is also one of the research priorities.

In order to reduce the simulation calculation time, scholars have proposed various calculation models to speed up calculation efficiency. The intrinsic strain method [17, 18] is a widely used physics-based method for fast prediction of part deformation and residual stress. However, it can neither capture the accumulation of thermal strain during heating, nor the layer-by-layer differential shrinkage of different layers. Accordingly, Liang et al. [2] improved the intrinsic strain method so that it can capture the accumulation of thermal strain during the heating process and improve the prediction accuracy of residual deformation. However, further research is needed to investigate the effect of complex forming trajectories and part geometries on the intrinsic strain method [2]. Adaptive grid technology is another way to improve computational efficiency. Li et al. [19] conducted weakly coupled thermo-mechanical simulations using an adaptive grid based on an octree coarse-graining technique, and the prediction accuracy was greater than 95%. Denlinger et al. [20] developed a hybrid approach combining a quiet inactive approach with adaptive mesh coarsening for large additively manufactured parts, predicting the deformation of a 3180-mm-long part with a maximum error of 29%. The third method is to use parallel computing. The iterative substructure method proposed by Murakawa [21] is proven to be 5–10 times faster than commercial software such as Abaqus. Huang et al. [1] developed an explicit finite element simulation method for wire arc additive manufacturing (WAAM) based on a graphics processing unit (GPU). They show that the GPU-based approach is effective in reducing the computational time. The fourth method is to apply the semi-analytical solution of the heat conduction equation under specific conditions to the stress field model, reducing the number of model solution steps and improving computational efficiency. Yang and Ayas [22] developed such a model and performed calculations for Ti6-Al4-V. In order to solve the problem of low solution efficiency caused by the small diameter of the heat source and the large number of layers, Hodge et al. [23] proposed an equivalent method to combine 20 physical layers into one finite element mesh layer while maintaining the ratio of laser size to powder layer height unchanged. Each of these methods has its own characteristics, but none of them has been verified on a large scale, and further verification is needed.

Based on the above research background, this paper simplifies the analytical solution of the heat conduction equation and develops a new temperature field model for the calculation of residual stress in AM. By removing the temperature field calculation in the thermal–mechanical coupling simulation process, the efficiency of additive manufacturing is improved. On this basis, the residual stress of the single-pass multi-layer cladding model was calculated and compared with the measured results, and the distribution characteristics of the residual stress in AM were studied.

## 2 Numerical calculation model

### 2.1 Solution process

The solution process of the method used in this study is shown in Fig. 1. The traditional AM residual simulation adopts sequentially coupled thermo-mechanical finite element method (SC-TM-FEM) or fully coupled thermo-mechanical finite element method (FC-TM-FEM). First, a geometric model needs to be established. Afterwards, preprocessing is performed on

**Fig. 1** Schematic diagram of the solution process
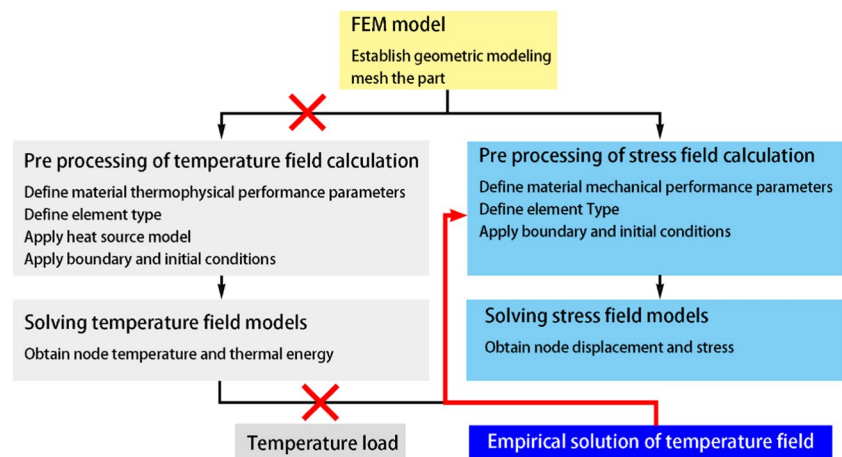
the temperature field calculation, including defining the thermophysical properties of the material, defining the element type, applying the heat source model, applying boundary conditions and initial conditions, and solving the temperature field to obtain the node temperature. Afterwards, the stress field model is pre-processed, including defining the thermophysical properties of the material, defining the element type and applying boundary conditions and initial conditions (temperature load). The solution efficiency is reduced and the difficulty of residual stress evaluation of large components manufactured by additive manufacturing is increased, since the model needs to be solved twice for the temperature field and the stress field. In this paper, we use the analytical solution of the temperature field of the semi-infinite body in [22] as a template to establish a simplified temperature field model. This temperature field is directly applied to the stress field model, and only the stress field model is solved to directly obtain the residual stress of additive manufacturing. Compared with the traditional method, the solution efficiency is improved with little loss of accuracy.

## 2.2 Temperature field model

Suppose there is a three-dimensional cube, and a laser is placed on top of it. The powder feeding nozzle attached to the laser feeds the powder into the upper surface of the cube, and the laser heats and melts the powder and part of the substrate. The lateral and bottom surfaces of the substrate are in contact with air. At time $t = 0$, the laser starts to move over the substrate along the cladding path, and the substrate and powder start to be heated, as shown in Fig. 2.

Under the assumptions of incompressibility, negligible viscosity and dissipation, linear relationship between heat flux and temperature gradient (Fourier's law), and no melt flow during solidification, the energy balance of each region of the substrate is governed by the classical energy balance equation.

$$\rho c_p \frac{\partial T}{\partial t} = \nabla(k\nabla T) + Q_v, \ in \ V \tag{1}$$

where $T$ is the temperature; $Q_v$ is the volumetric heat generation rate; $\rho$, $c_p$, and $k$ are the density, specific heat capacity at constant pressure, and thermal conductivity coefficient, respectively. During the SLM process, the temperature of the base plate is usually kept at a constant value. The bottom surface is therefore set to a fixed temperature.

If the material parameters $\rho$, $c_p$, and $k$ are assumed to be independent of temperature, Eq. (1) becomes a linear heat conduction equation which can be solved using the superposition principle. Jaeger and Carslaw [24] gave the analytical solution for a single-point heat source in a semi-infinite space as

$$T_p\left(x_i, t\right) = \frac{QA}{4\rho c_p(\pi\alpha(t - t_0 + t_r))^{3/2}}\exp(\frac{-R^2}{4\alpha(t - t_0 + t_r)}) \tag{2}$$

where $Q$ represents the energy associated with the heat source, and the determination of the absorption rate $A$ is detailed in [25]. $\alpha = k/\rho c_p$ represents the thermal diffusivity. $t_0$ represents the initial time of heat source activation, and $t_r = r_1/8\alpha$ is used to eliminate the singularity at $t = t_0$. The expression $t_r$ indicates that the point heat source has spread over a distance $r_1$. $R$ represents the distance from the point heat source to the material point $x_i$. If the number of point heat sources representing a scan line is large enough, the energy $Q$ given in Eq. (2) can be expressed by $Q = P\Delta t$, where $P$ is the laser power and $\Delta t$ is the time step. It can be seen that the laser heat source is Gaussian distributed in the spatial domain.

In order to simplify the model and improve calculation efficiency, we simplify the temperature field around the heat source into the following formula,

$$T = \begin{cases} T_i exp\left(-3\left(\frac{x}{a}\right)^2 - \left(\frac{y}{b}\right)^2 - \left(\frac{z}{c_f}\right)^2\right) + T_m \\ T_i exp\left(-3\left(\frac{x}{a}\right)^2 - \left(\frac{y}{b}\right)^2 - \left(\frac{z}{c_r}\right)^2\right) + T_m \end{cases} \tag{3}$$

**Fig. 2** Schematic diagram of SLM process
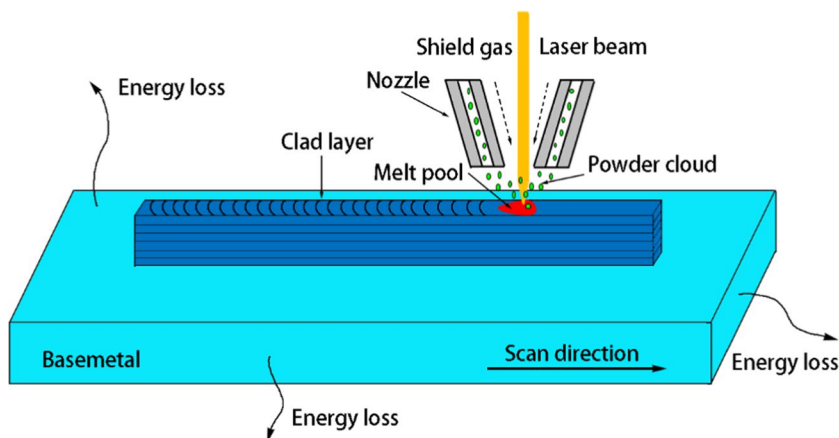
where, $a$, $b$, $c_f$ and $c_r$ are heat source parameters respectively, and $T_i$ represents the peak temperature in the molten pool. Assuming that the laser energy acts on the inside of the molten pool, the relationship between $T_i$ and the total laser energy $Q$ satisfies the following formula:

$$Q\eta = Sv\rho(c_p(T_i - T_m) + \Delta H_m) \tag{4}$$

where $\eta$ is the energy coefficient entering the substrate; $S$ is the cross-sectional area of the molten pool; $v$ is the welding speed; $\rho$ is the density of the substrate; $c_p$ is the specific heat capacity of the substrate at constant pressure; $\Delta H_m$ is the specific heat of melting of the clad melt; and $T_m$ is the temperature of the substrate. Assuming that the energy absorbed by the substrate tends to be uniformly distributed to the interior of the printed part during the subsequent cooling process, after a certain time ($t$), the relationship between $T_m$ and the total laser energy $Q$ satisfies the following formula:

$$Q\eta t_0 - h(T_m - T_{m0})t = \rho V C_p(T_m - T_{m0}) \tag{5}$$

where $t_0$ is the laser action time, and $T_{m0}$ is the initial temperature of the substrate.

## 2.3 Stress field model

The stress–strain field of AM is formed under the action of the laser heat source, the internal stress caused by the uneven heating of the workpiece and the external stress introduced by the fixture. A high-energy–density laser melts powder and a portion of the base metal to form a molten pool. The thermal expansion of the unmelted base metal adjacent to the molten pool is different under the unevenly distributed temperature field, thus forming compressive internal stress. During the cooling process, the shrinkage of each part near the molten pool is different, and at the same time, it is limited by the surrounding materials and is in a state of tension. After cooling to room temperature, residual stress is formed [26].

Since the thermal stress generated during the AM process is generally greater than the yield stress of the material, the thermoelastic-plastic theory is used to calculate the residual stress and deformation during the additive manufacturing process. This method associates the temperature change with the deformation of the object, so that the stress and strain of the object due to the local temperature gradient can be obtained through the temperature change. Geometry and material non-linearity are involved in the stress–strain calculation of AM. It is very difficult to solve these non-linear problems. In order to simplify the calculation, it is regarded as a material and geometric non-linear transient problem and the following assumptions are made [27]:

1. The viscosity and creep phenomena of the material are not considered.
2. All materials comply with the von Mises yield criterion.

3. The elasticity, plasticity, and temperature strain of materials during heating and cooling are inseparable.
4. After the material yields, the flow behavior conforms to the isotropic strengthening criterion.
5. Stress, strain, and thermal energy are linear in the solution time interval.

SLM welding seam and heat-affected zone will produce elasticity, plastic deformation, and volume change under the action of high-density heat. When solving by the finite element method, the displacement increment of the nodes needs to be calculated first, and then the stress increment is calculated according to the constitutive equation. The stress–strain relationship and element balance equation of the material in the elastic and plastic stages are shown in Eqs. (6) and (7) [28]:

$$d\sigma = Dd\varepsilon - CdT \tag{6}$$

$$dF^e + dR^e = K^e d\delta^e \tag{7}$$

where $d\sigma$ represents stress increment (MPa); $d\varepsilon$ represents strain increment; $dT$ represents temperature increment; $D$ represents elastic or plastic stiffness matrix; $C$ represents temperature-related vector; $dF^e$ represents node external force increment; $dR^e$ represents the increment of the equivalent nodal force of the initial strain element; $K^e$ represents the element stiffness matrix; and $d\delta^e$ represents the nodal displacement increment.

## 2.4 Calibration and verification of model parameters

During the test, AM900 nickel-based superalloy powder was used for SLM. The actual cladding process (with parameters listed in Table 1) was carried out on an industrial robot with a fiber laser, as shown in Fig. 3 (a). First, a single-pass single-layer cladding test (Fig. 3 (b)) was carried out, and the molten pool profile was obtained, as shown in Fig. 3 (c). Afterwards, a single-pass multi-layer cladding test was carried out, and the molten pool profile was obtained, as shown in Fig. 3 (d).

First, a single-channel single-layer accumulation experiment is carried out, and the penetration depth (a) and half-melt width (b) in formula (3) are obtained by metallographic analysis method, assuming that $c_r$ is the half-melt width, and $c_f$ is 4 times the half-melt width. According to the welding process parameters and the material properties of AM900 alloy, as shown in Fig. 4, $T_i$ is calculated by formula (4), and $T_m$ is calculated by formula (5). The obtained temperature field model is input into the stress field model as a load. In the stress field model, the elastic behavior of materials is simulated by isotropic Hooke's law. The effect

**Table 1** Laser cladding process parameters

| Parameter | Value |
|---|---|
| Laser power | 700 (W) |
| Scanning speed | 0.01 (m/s) |
| The powder feeding rate | 7.8 (g/s) |
| The focal length of the laser | 20 (mm) |
| Protection gas (Ar) | 15 (L/min) |
| The powder feeding gas (Ar) | 7 (L/min) |
| Laser spot diameter | 2.4 (mm) |

of temperature on the mechanical behavior is taken into account through the coefficient of thermal expansion. For plastic behavior, a rate-independent plasticity model is used. The von Mises yield criterion is used to simulate the material yielding, and the isotropic hardening model is used to simulate the flow behavior of the material after yielding. By setting the plastic strain of the material above the melting temperature to zero, the hardening history is cleared to more accurately simulate the residual stress in the molten pool [29].



**Fig. 3** Experimental process: **a** cladding process; **b** single-pass single-layer cladding layer; **c** the molten pool profile of single-pass single-layer cladding; **d** the molten pool profile of single-pass multi-layer cladding
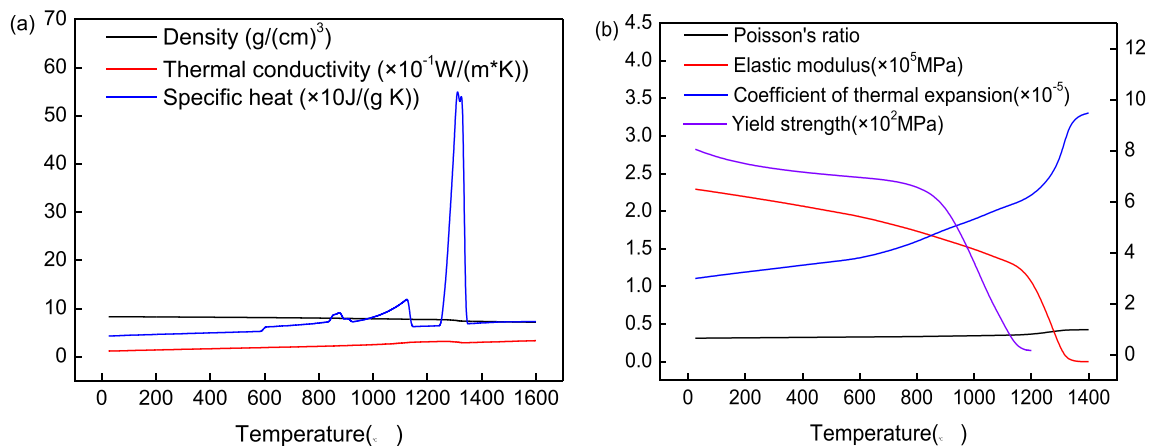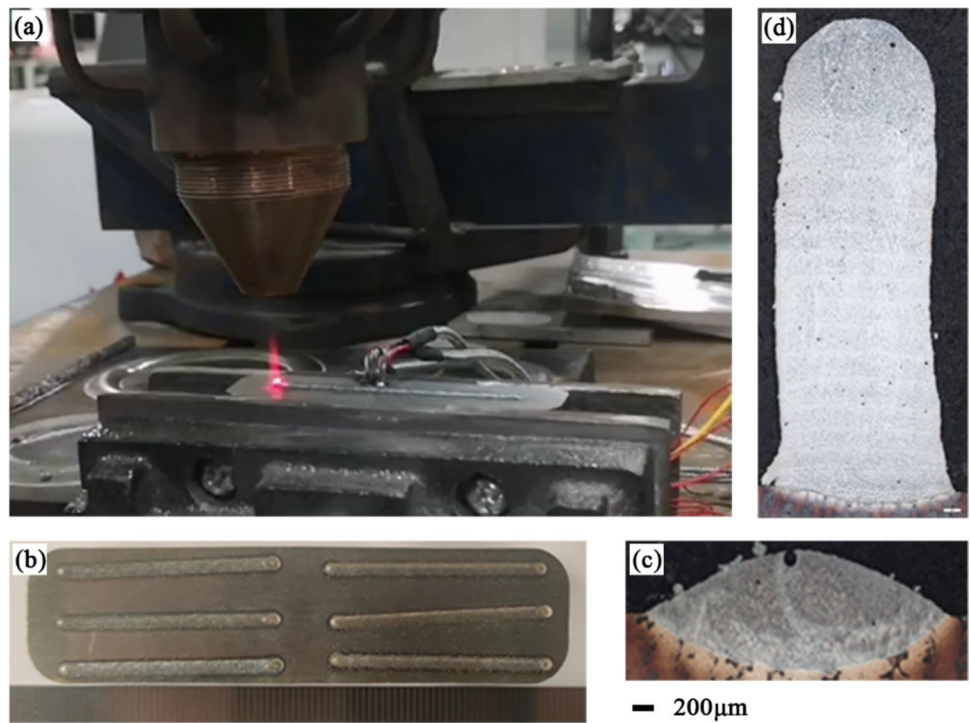


**Fig. 4** Material properties of AM900 changing with temperature: **a** thermal physical properties; **b** mechanical properties
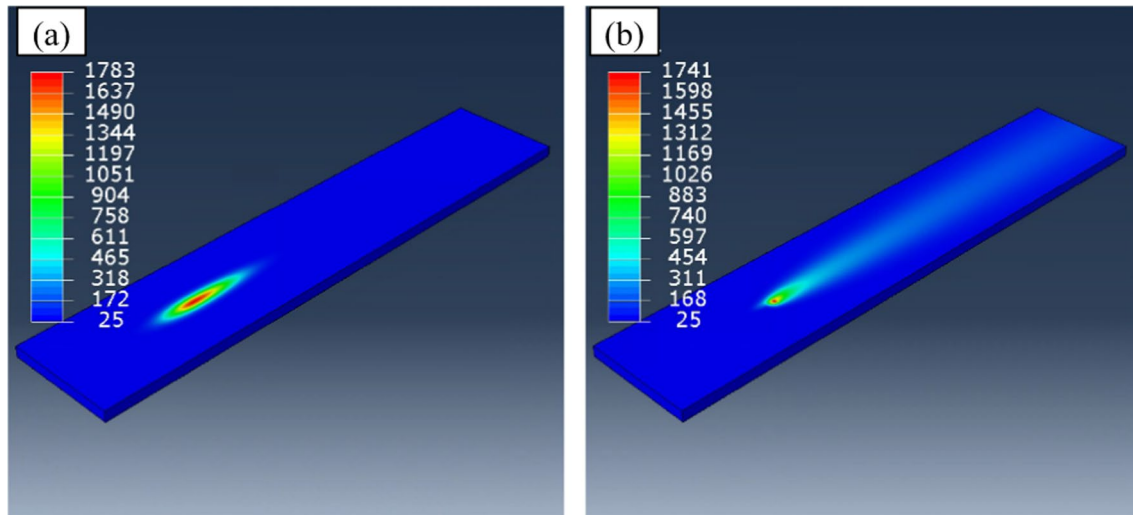
**Fig. 5** Comparison of temperature field: **a** the method used in this study; **b** the traditional thermal–mechanical coupling finite element method

In this study, the traditional thermal–mechanical fully coupled finite element calculation was first performed on the SLM single-pass single-layer cladding to calculate residual stress, and then the simplified method was used. The calculation accuracy and efficiency of the two methods were compared. Afterwards, the simplified method is used to calculate the single-pass multi-layer residual stress and compare it with the measured residual stress.

The contour method was first proposed by Prime, a research engineer at Los Alamos National Laboratory (LANL), in 2000 at the Sixth International Residual Stress Conference [30]. This method has the advantages of simple theory, simple test process, and high test accuracy, and has been widely used in stress tests of industrial structural parts such as aviation, aerospace, and nuclear power. The contour method has been widely used in the residual stress test of various materials after more than 10 years of development and improvement, and it is currently the most accurate destructive testing technology. In this study, the contour

method was used to measure the residual stress distribution of single-pass multi-layer samples.

# 3 Results and discussion

## 3.1 Comparison with the traditional thermodynamic fully coupled model

In order to illustrate the effectiveness of this model in simulating the AM residual stress, firstly, this model and the traditional thermal–mechanical coupling finite element method are used to model the SLM single-pass single-layer cladding on a $200 \times 50 \times 4$-mm plate, and the obtained temperature field is shown in Fig. 5. It can be seen from the figure that the temperature distribution and maximum temperature of the two models are relatively similar. However, the temperature drop behind the molten pool in this model is faster than that of the traditional thermal–mechanical coupling finite

**Fig. 6** Comparison of transverse residual stress: **a** the method used in this study; **b** the traditional thermal–mechanical coupling finite element method
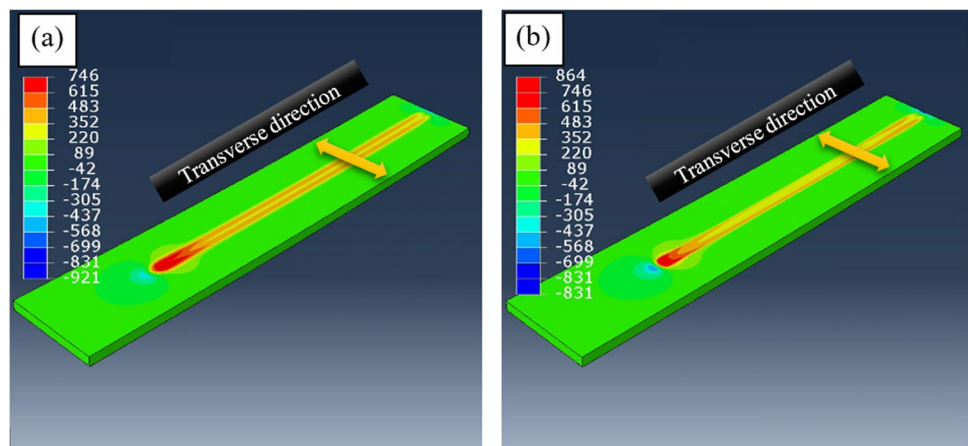
**Fig. 7** Comparison of longitudinal residual stress: **a** the method used in this study; **b** the traditional thermal–mechanical coupled finite element method
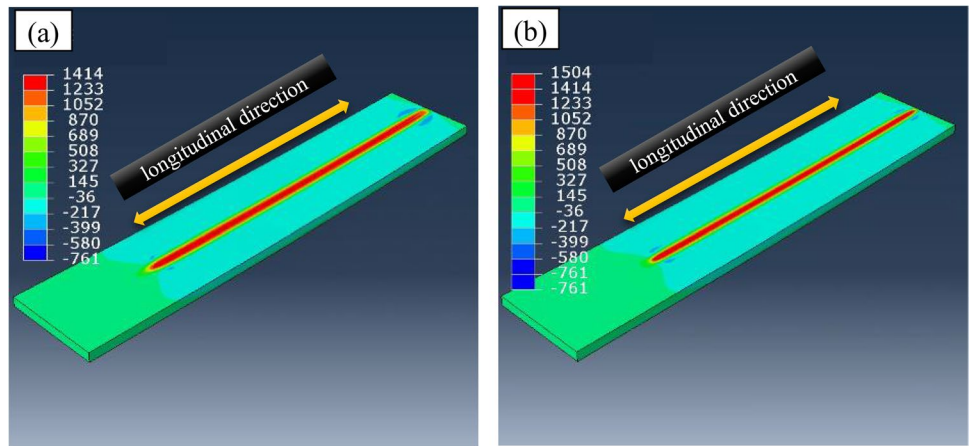


**Fig. 8** Comparison of maximum principal plastic strain: **a** the method used in this study; **b** the traditional thermal–mechanical coupling finite element method
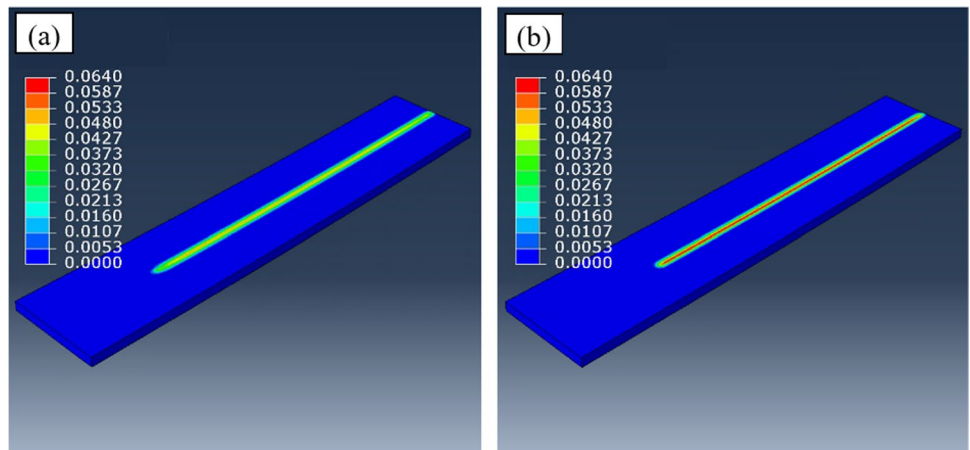
element method. This is mainly because the time term is not considered in the applied temperature field (formula 3), so the model cannot account for the energy transport, convection and radiation increasing with time, so the temperature is lower behind the molten pool.

Next, the transverse residual stresses (perpendicular to the welding direction) of the models were compared, and the results are shown in Fig. 6. It can be seen from the figure that the distribution laws of the transverse residual stress of the two models are the same. The maximum value of

transverse residual stress predicted by the method adopted in this study is reduced by 13% compared with the traditional thermal–mechanical coupling finite element method.

Figure 7 compares the longitudinal residual stresses (parallel to welding direction) of the models. It can be seen from the figure that the distribution laws of the longitudinal residual stress of the two models are also the same. The maximum value of longitudinal residual stress predicted by the method adopted in this study is reduced by 5.98% compared with the traditional thermal–mechanical coupling finite element method.
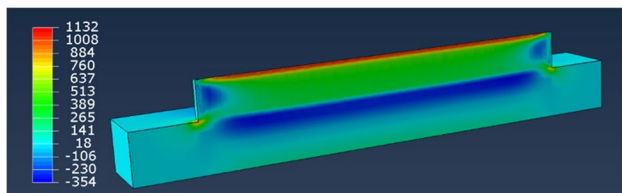


**Fig. 9** Residual stress along the scanning direction of single-pass multi-layer cladding
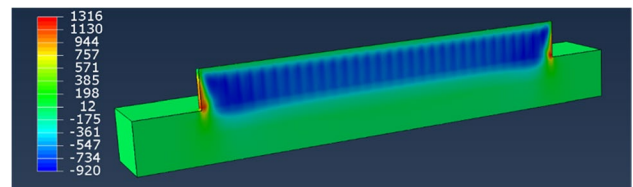


**Fig. 10** Residual stress along the printing height direction of single-pass multi-layer cladding

**Fig. 11** Comparison of simulation and test: **a** residual stress along the scanning direction measured by the contour method; **b** residual stress along the scanning direction simulated by finite element method; **c** residual stress along the path direction
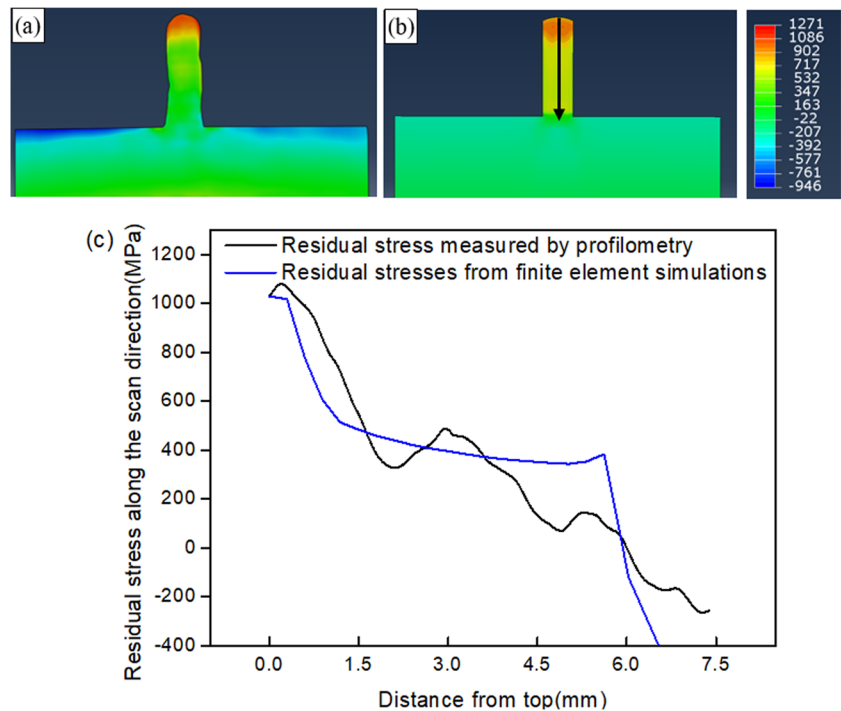


Figure 8 compares the maximum principal plastic strains of the models. It can be seen from the figure that the distribution law of the maximum principal plastic strain of the two models is also the same. However, the plastic strain calculated by the method used in this study is small and the distribution is narrow.

Although the model developed in this study has a lower temperature behind the weld pool compared to the traditional thermal–mechanical coupled finite element method, it does not affect its ability to predict post-weld residual stress. This is mainly because, for materials that have not undergone a solid-state phase transition, the coefficient of thermal expansion is an approximately linear function, and the residual stress upon cooling to room temperature is only related to the highest temperature experienced without considering external constraints. Through the above analysis, it can be concluded that the model established in this study can reflect the residual stress of laser powder feeding single-layer single-pass cladding, and a more accurate model can be obtained through verification with experiments and finite element models. The biggest advantage of this model is the calculation efficiency. By comparing with the traditional thermal–mechanical coupled finite element method, the method used in this study needs 2.8 h to complete the calculation, while the traditional thermal–mechanical coupled finite element method needs 18.467 h to complete the calculation when using the same hardware for calculation. The method employed in this study is 5.6 times faster than the conventional thermomechanical coupled finite element method. By observing the calculation results, it is found that the traditional thermal–mechanical

coupling finite element method has poor convergence and requires more solution steps. Therefore, a method to improve the efficiency of finite element simulation for SLM is proposed. First, the method used in this study was corrected by using the traditional finite element method for single-pass single-layer simulation, while measuring the thermal cycle curve and residual stress during the test. Then, the method of this study is used to simulate the residual stress of multi-pass multi-layer SLM.

### 3.2 Single-pass multi-layer residual stress distribution

A single-pass multi-layer cladding was modeled using the method described above, and a total of 20 layers were deposited. The obtained residual stress along the scanning direction is shown in Fig. 9. It can be seen from the figure that the position with the largest residual stress appears at the end of the uppermost layer of the sample. At the same time, the position where the printed body is combined with the substrate is the position where the stress concentration is relatively serious. The middle position on the upper surface of the substrate shows compressive stress.

Figure 10 shows the deposited participating stress along the printing height direction. At this time, the inside of the sample shows compressive stress and the two sides show tensile stress, and the value of the tensile stress is relatively high. The distribution law of the residual stress is similar to the distribution law of the low carbon steel sample measured by neutron diffraction in the literature [31].

## 3.3 Model validation

The residual stress of the sample is measured by the contour method, as shown in Fig. 11 (a), and the residual stress of the finite element simulation is shown in Fig. 11 (b). The residual stress on the path of the black arrow shown in Fig. 11 (b) is plotted, and the obtained results are shown in Fig. 11 (c). It can be seen from the figure that the simulated results are basically consistent with the measured results, indicating the correctness of the model. Although the model can capture the trend of residual stress distribution, there is still a certain gap in the value of residual stress at the position where the printed body contacts the substrate.

## 4 Conclusion

In this paper, the analytical solution of the heat conduction equation is simplified, and a new temperature field model for the calculation of residual stress in additive manufacturing is developed, which simplifies the calculation of the temperature field in the thermal–mechanical coupling simulation process, thereby improving the efficiency of additive manufacturing. On this basis, the residual stress of the single-pass multi-layer cladding model was calculated and compared with the measured results, and the distribution characteristics of the residual stress in SLM were studied. The following conclusions were obtained:

1. The established model is closed to the result of thermal–mechanical coupling finite element method.
2. The established model can reflect the residual stress of the SLM process.
3. Compared with the traditional thermal–mechanical coupling finite element method, the calculation efficiency of the model established in this study is greatly improved.

## Declarations

**Conflict of interest** The authors declare no competing interests.

## References

1. Huang H, Ma N, Chen J et al (2020) Toward large-scale simulation of residual stress and distortion in wire and arc additive manufacturing. Addit Manuf 34:101248
2. Liang X, Cheng L, Chen Q et al (2018) A modified method for estimating inherent strains from detailed process simulation for fast residual distortion prediction of single-walled structures fabricated by directed energy cladding. Addit Manuf 23:471–486
3. Jimenez X, Dong W, Paul S et al (2020) Residual stress modeling with phase transformation for wire arc additive manufacturing of B91 steel. Jom 72:4178–4186
4. Lee Y, Bandari Y, Nandwana P et al (2019) Effect of interlayer cooling time, constraint and tool path strategy on deformation of large components made by laser metal cladding with wire. Appl Sci 9(23):5115
5. Nycz A, Noakes MW, Richardson B et al (2017) Challenges in making complex metal large-scale parts for additive manufacturing: a case study based on the additive manufacturing excavator. International Solid Freeform Fabrication Symposium. University of Texas at Austin
6. Song X, Feih S, Zhai W et al (2020) Advances in additive manufacturing process simulation: residual stresses and distortion predictions in complex metallic components. Mater Des 193:108779
7. Walker D (2001) Residual stress measurement techniques. Adv Mater Processes 159(8):30–30
8. Li C, Liu ZY, Fang XY et al (2018) Residual stress in metal additive manufacturing. Procedia Cirp 71:348–353
9. Chen Y, Liu Y, Chen H et al (2022) Multi-scale residual stress prediction for selective laser melting of high strength steel considering solid-state phase transformation. Opt Laser Technol 146:107578
10. Weisz-Patrault D (2020) Fast simulation of temperature and phase transitions in directed energy deposition additive manufacturing. Addit Manuf 31:100990
11. Ahn J, He E, Chen L et al (2017) Prediction and measurement of residual stresses and distortions in fibre laser welded Ti-6Al-4V considering phase transformation. Mater Des 115:441–457
12. Mirkoohi E, Li D, Garmestani H et al (2021) Residual stress modeling considering microstructure evolution in metal additive manufacturing. J Manuf Process 68:383–397
13. Mukherjee T, Zhang W, DebRoy T (2017) An improved prediction of residual stresses and distortion in additive manufacturing. Comput Mater Sci 126:360–372
14. Fallah V, Alimardani M, Corbin SF et al (2011) Temporal development of melt-pool morphology and clad geometry in laser powder cladding. Comput Mater Sci 50(7):2124–2134
15. Walker TR, Bennett CJ, Lee TL et al (2020) A novel numerical method to predict the transient track geometry and thermomechanical effects through in-situ modification of the process parameters in Direct Energy Cladding. Finite Elem Anal Des 169:103347
16. Wolff SJ, Gan Z, Lin S et al (2019) Experimentally validated predictions of thermal history and microhardness in laser-deposited Inconel 718 on carbon steel. Addit Manuf 27:540–551
17. Ueda Y, Fukuda K, Tanigawa M (1979) New measuring method of three dimensional residual stresses based on theory of inherent strain. Trans Jpn Weld Res Inst 8(2):249–256
18. Deng D, Murakawa H, Liang W (2007) Numerical simulation of welding distortion in large structures. Comput Methods Appl Mech Eng 196(45–48):4613–4627
19. Li C, Denlinger ER, Gouge MF et al (2019) Numerical verification of an Octree mesh coarsening strategy for simulating additive manufacturing processes. Addit Manuf 30:100903
20. Denlinger ER, Irwin J, Michaleris P (2014) Thermomechanical modeling of additive manufacturing large parts. J Manuf Sci Eng 136(6)
21. Murakawa H, Ma N, Huang H (2015) Iterative substructure method employing concept of inherent strain for large-scale welding problems. Weld World 59:53–63
22. Yang Y, Ayas C (2017) Computationally efficient thermal-mechanical modelling of selective laser melting. AIP Conference Proceedings. AIP Publishing LLC 1896(1):040005

23. Hodge NE, Ferencz RM, Vignes RM (2016) Experimental comparison of residual stresses for a thermomechanical model for the simulation of selective laser melting. Addit Manuf 12:159–168

24  Jaeger JC, Carslaw HS (1959) Conduction of heat in solids. Clarendon P, Oxford

25. Robert A, Debroy T (2001) Geometry of laser spot welds from dimensionless numbers. Metall and Mater Trans B 32:941–947

26. Yucang W, Xiangjie W (2012) Effect of welding residual stress and deformation in CO2 gas shielded welded joints of Q345D steel. Hot Work Technol 41:151–154

27. Yongfeng Zou (2017) Numerical simulation and experimental research on welding residual stress of thick plate for steel bridge. Southwest Jiaotong University

28. Zhao Q, Wu C (2012) Numerical analysis of welding residual stress of U-RIB stiffended plate. Engineering Mechanics 8(29):262–268

29. Yu D, Yang C, Sun Q et al (2023) Impact of process parameters on temperature and residual stress distribution of X80 pipe girth welds. Int J Press Vessels Pip 203:104939

30. Prime MB, Gonzales AR (2000) The contour method: simple 2-D mapping of residual stresses. Proceeding of 6th International conference on residual stresses, Oxford, U.K., 1:617–624

31. Nycz A, Lee Y, Noakes M et al (2021) Effective residual stress prediction validated with neutron diffraction method for metal large-scale additive manufacturing. Mater Des 205:109751